Journal of Rock Mechanics and Geotechnical Engineering 14 (2022) 922–935

Contents lists available at ScienceDirect

Journal of Rock Mechanics and Geotechnical Engineering

journal homepage: www.jrmge.cn

Full Length Article

An undrained expansion solution of cylindrical cavity in SANICLAY for K_0-consolidated clays

Haohua Chen [a,b], Pin-Qiang Mo [a,*]

[a] China University of Mining and Technology, Xuzhou 221116, China
[b] The University of Arizona, Tucson, AZ 85716, USA

ARTICLE INFO

Article history:
Received 9 July 2021
Received in revised form
6 September 2021
Accepted 18 October 2021
Available online 8 January 2022

Keywords:
Undrained cavity expansion
SANICLAY
K_0-consolidation
Anisotropy

ABSTRACT

This paper proposes a rigorous undrained solution for cylindrical cavity expansion problems in K_0-consolidated clays, adopting a simple non-associated and anisotropic model, SANICLAY. The cavity expansion theory is well extended to consider non-associativity, K_0-consolidation and stress-induced anisotropy with combined rotational and distortional hardening of yield surface and plastic potential in the multiaxial stress space. The developed solution can be recovered for validation against the modified Cam-clay (MCC) solution by simply setting model constants, avoiding non-associativity and anisotropy. The source code is provided to facilitate the use for extensions. After investigating the effects of overconsolidation ratio on the cavity pressure curves, stress distributions, evolutions of anisotropic parameters and stress paths, the variations with three-dimensional (3D) evolutions of yield surface and plastic potential during undrained cavity expansion are shown for various K_0-consolidated clays. A parametric study on the model constants is presented to depict the influences on the stress distributions and paths, critical state surfaces and Lode's angles at failure. The proposed solution also provides a general framework for formulating equations for undrained expansion of cylindrical cavities under an initial cross anisotropic condition using sophisticated anisotropic soil models. It serves as a precise benchmark for extensions of analytical solutions, numerical simulations of cavity expansion, and back-calculations of geotechnical problems.

1. Introduction

The in situ stress state of natural soil deposits is usually inherently anisotropic, and it is common to define the at-rest coefficient as the ratio of horizontal (σ'_{h0}) to vertical (σ'_{v0}) effective stress at the geostatic condition, i.e. $K_0 = \sigma'_{h0}/\sigma'_{v0}$. Considering the sedimentary process without lateral deformation, the initial stress-induced anisotropy is particularly crucial to the mechanical behaviours of saturated clays (e.g. Nakase and Kamei, 1983; Ghaboussi and Momen, 1984; Mayne, 1985; Wang et al., 2008). Following the early developments on plasticity theory for geomaterials, many anisotropic constitutive models for soft clays have been proposed considering anisotropic K_0-consolidation. Originated from the anisotropic extension of work by Dafalias (1986), the anisotropic critical state models were extensively developed with various types of yield surfaces and hardening rules (e.g. Whittle and Kavvadas, 1994; Wheeler et al., 2003; Dafalias et al., 2006; Yin et al., 2010; Rezania et al., 2016). The SANICLAY (an abbreviation of 'Simple ANIsotropic CLAY') model, extended by Dafalias et al. (2006), is one of the milestones for simulation of both undrained and drained rate-independent behaviours of sensitive clays, using a non-associated flow rule, a combined rotational and distortional hardening rule and the evolution laws for hardening variables. Extensions of the SANICLAY model have also been developed in the recent years for further considerations of destructuration, plastic deformations within yield surface, and cyclic behaviour, etc. (e.g. Taiebat et al., 2010; Jiang et al., 2012; Dafalias and Taiebat, 2013; Seidalinov and Taiebat, 2014; Yang et al., 2019).

The cavity expansion theory has been greatly developed and widely applied in geotechnical engineering since 1940s (e.g. Bishop et al., 1945; Hill, 1950; Chadwick, 1959). Considering more sophisticated constitutive models for geomaterials, cavity expansion solutions have been progressively improved during the past half century (e.g. Vesic, 1972; Carter et al., 1986; Yu and Houlsby, 1991;

* Corresponding author.
E-mail address: pinqiang.mo@cumt.edu.cn (P.-Q. Mo).
Peer review under responsibility of Institute of Rock and Soil Mechanics, Chinese Academy of Sciences.

https://doi.org/10.1016/j.jrmge.2021.10.016

Cao et al., 2001; Chen and Abousleiman, 2012; 2018; Mo and Yu, 2017, 2018; Chen et al., 2020; Zhao et al., 2020). The derivations for stress and displacement fields around cavities are then employed for analyses of complex geotechnical problems, including in situ soil testing, foundations, underground excavations, wellbore instability. However, most of the early solutions are developed for cavities embedded in an infinite medium and isotropic stress field, leading to inaccurate results for solving boundary value problems in numerous applications. Correction factors based on numerical methods or empirical relationships were then introduced for the compromised use of analytical results (e.g. Naggar and Naggar, 2012).

Over the last decade, many attempts have been made to tackle this issue providing semi-analytical solutions of cavity expansion or contraction under anisotropic initial stress conditions. Following the framework of Chen and Abousleiman (2012, 2013), semi-analytical solutions of undrained and drained cylindrical cavity expansion were proposed by Li et al. (2016a, 2017) to consider the effects of initial stress anisotropy by employing an associative K_0-consolidated anisotropic modified Cam-clay (AMCC) model (Sekiguchi and Ohta, 1977). It was reported that the degree of initial anisotropy has a notable influence on the stress distributions around the cylindrical cavity, though the rotation of yield surface representing the stress-induced anisotropy was neglected for simplicity. Chen and Liu (2019) reported a rigorous undrained solution in the AMCC model (Dafalias, 1987), which considers both rotation and distortion of yield surfaces. The effects of K_0-consolidation and the stress-induced anisotropy were clearly shown on the distributions of effective stresses and excess pore pressure around the cylindrical cavity. This work was then extended for the drained solution (Liu and Chen, 2018). Similarly, an undrained solution in the S-CLAY1 model (Wheeler et al., 2003) was developed by Sivasithamparam and Castro (2018), considering the fabric anisotropy of soft soils and its evolution with plastic strains. It was later updated using the S-CLAY1S model (Karstunen et al., 2005), accounting for both fabric anisotropy and destructuration (Sivasithamparam and Castro, 2020).

Since the strength of clay is typically overestimated by the Mises criterion-based models, the spatially mobilized plane (SMP) criterion is suggested for the three-dimensional (3D) strength of the cohesive-frictional soil (Li et al., 2016b). Following the advanced cavity expansion solutions of Li et al. (2016b) and Chen and Abousleiman (2012), Chen et al. (2019) presented a generic stress transform approach for both undrained and drained cylindrical cavity expansion solutions in an SMP criterion revised AMCC model (Yao and Wang, 2014). The solution was then modified for the undrained contraction problems by Zhang et al. (2020). Additionally, the effects of rotational hardening, ignored in Chen et al. (2019), have been recently included in Yang et al. (2020) under drained loading conditions. Some recent solutions for cavity expansion theory are summarized and compared in Table 1.

In this paper, an undrained expansion solution in the SANICLAY model, incorporating 3D strength of soil, a non-associated flow rule and a combined rotational and distortional hardening rule, is proposed for cylindrical cavities considering K_0-consolidation and stress-induced anisotropy. The solution with attached corresponding MATLAB source code (see Appendix A) is validated against that based on the recovered isotropic model by Chen and Abousleiman (2012), and the results of K_0-consolidated clays are presented to investigate the effects of overconsolidation ratio and model constants on the cavity expansion responses and the stress paths, along with the evolutions of anisotropic parameters. The highlight of this context also lies in the provided generic framework for the derivation of undrained cavity expansion in an anisotropic critical state model, and the solution using the SANICLAY model could serve as a useful benchmark for further developments and numerical calculations, along with the source code and a worked-out example.

Table 1
Summary of recent solutions to cavity expansion problem.

Constitutive model	Predominant features	Source
Modified Cam-clay (MCC)	–	Chen and Abousleiman (2012, 2013)
K_0-consolidated anisotropic MCC	K_0-consolidation	Li et al. (2016a, 2017)
ACMEG-T (Laloui and François, 2009)	Environmental geomechanical thermal effect	Zhou et al. (2017)
Unified state parameter model	Overall soil (sand and clay) behaviour	Mo and Yu (2017, 2018)
SMP revised AMCC	K_0-consolidation and 3D strength	Chen et al. (2019)
Anisotropic MCC model (Dafalias, 1987)	K_0-consolidation and the stress-induced anisotropy	Chen and Liu (2019); Liu and Chen (2018)
S-CLAY1 model (Wheeler et al., 2003)	K_0-consolidation and the stress-induced anisotropy	Sivasithamparam and Castro (2018); Chen et al. (2020)
EVP constitutive model (Kelln et al., 2008)	Elastic-viscoplastic behavior of soil	Zhou et al. (2020)
SMP revised S-CLAY1	K_0-consolidation, anisotropy, and 3D strength	Yang et al. (2020)
Modified Cam-clay (MCC)	Similarity solving technique	Zhou et al. (2021)
Einav's breakage mechanics model (Einay, 2007)	Crushable soils	Liu et al. (2021)

2. Definition of cavity expansion problem

The problem of this study concerns with the evolutions of stress and displacement fields during the undrained expansion of a vertical and cylindrical cavity in K_0-consolidated clays. Assuming the plane-strain condition along the vertical direction, the in-plane schematic of the cylindrical cavity expansion problem is illustrated in Fig. 1. The initial stress condition of the infinite soil mass is considered as K_0-consolidated with in situ horizontal and vertical effective stresses σ'_{h0} and σ'_{v0}. The case $\sigma'_{r0} \neq \sigma'_{\theta 0}$ will not be considered in the present

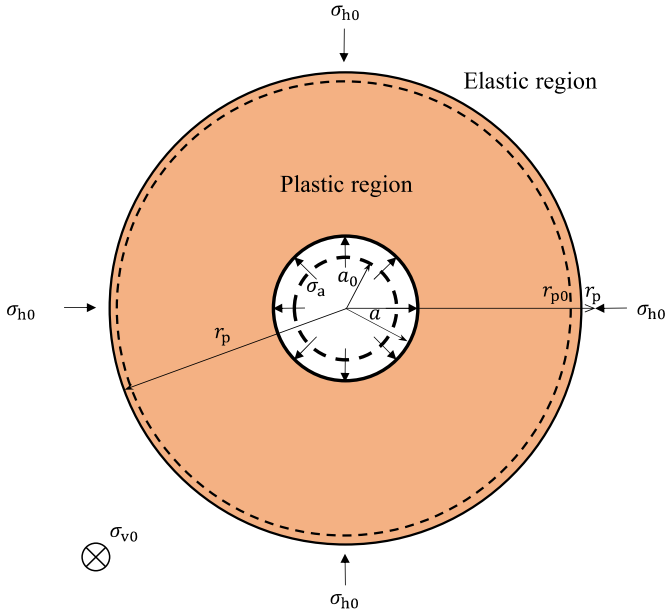

Fig. 1. Schematic illustration of cylindrical cavity expansion problem.

study, in which σ'_{r0} and $\sigma'_{\theta 0}$ are the initial radial and circumferential stresses, respectively. The circular cavity expands from its initial cavity radius a_0 to its current cavity radius a under an internal cavity pressure σ_a. During the process of expansion, soil mass near the cavity wall is squeezed outwards under the increase of internal cavity pressure, and a plastic region with a radius of r_p is developed around the cavity wall, which is embedded within the outer elastic region. In the framework of critical state soil mechanics, further expansion may create a critical state region adjoined to the cavity wall. The quasi-static stress state of an arbitrary soil element around the cylindrical cavity at any time is governed by the equilibrium equation in the radial direction alone:

$$\frac{\mathrm{d}\sigma'_r}{\mathrm{d}r}+\frac{\mathrm{d}u}{\mathrm{d}r}+\frac{\sigma'_r-\sigma'_\theta}{r}=0 \tag{1}$$

where σ'_r and σ'_θ are the effective radial and circumferential stresses, respectively; u is the pore water pressure; r is the radius of a soil element; d() is the Eulerian derivative for every material particle at a specific moment.

To accommodate large strains in the plastic and critical state regions during the cavity expansion process, the logarithmic strains are assumed as (Chen and Abousleiman, 2012; Chen et al., 2021):

$$\varepsilon_r=-\ln\left(\frac{\mathrm{d}r}{\mathrm{d}r_0}\right) \tag{2a}$$

$$\varepsilon_\theta=-\ln\left(\frac{r}{r_0}\right) \tag{2b}$$

where ε_r and ε_θ are the radial and circumferential strains, respectively; r_0 is the initial position of a soil element before expansion. The undrained expansion condition used to formulate the problem later indicates that the specific volume v remains constant during expansion, and the volumetric strain ε_v of soil around the cavity vanishes everywhere, which gives

$$\varepsilon_v=\varepsilon_r+\varepsilon_\theta+\varepsilon_z=\varepsilon_r+\varepsilon_\theta=0 \tag{3}$$

where ε_z is the vertical strain, which is equal to zero under the plane-strain condition.

3. SANICLAY model

The fundamental formulation of the SANICLAY model developed by Dafalias et al. (2006) will be adopted in the present solution. The tensorial form of the plastic potential in the general stress space is given as

$$g=\frac{3}{2}(\boldsymbol{s}-p'\boldsymbol{\alpha}):(\boldsymbol{s}-p'\boldsymbol{\alpha})-\left(M^2-\frac{3}{2}\boldsymbol{\alpha}:\boldsymbol{\alpha}\right)p'(p'_\alpha-p')=0 \tag{4}$$

where $\boldsymbol{s}$ is the deviatoric stress tensor, defined as $\boldsymbol{s}=\boldsymbol{\sigma}-p'\boldsymbol{I}$ ($\boldsymbol{\sigma}$ is the effective stress tensor, $\boldsymbol{I}$ is the identity tensor, and p' is the effective mean stress with $p'=(1/3)\mathrm{tr}\boldsymbol{\sigma}$); $\boldsymbol{\alpha}$ is the non-dimensional anisotropic variable tensor, which serves for the rotational hardening of the plastic potential surface; the symbol ':' implies the trace of the product of two tensors; M is the critical stress ratio; p'_α is the value of p' at $q=p'\alpha$, where q is the deviatoric stress and $\alpha=[(3/2)\boldsymbol{\alpha}:\boldsymbol{\alpha}]^{1/2}$. It should be noted that p'_α is determined by substituting the tensors $\boldsymbol{s}$ and $\boldsymbol{\alpha}$ into Eq. (4), and no hardening law is adopted to updated p'_α. In the general stress space, the 3D soil strength is considered by means of the Lode's angle θ_L, and the Lode's angle dependent formulation of M is defined as follows:

$$M=\frac{2M_e/M_c}{(1+M_e/M_c)-(1-M_e/M_c)\cos(3\theta_L)}M_c \tag{5a}$$

$$\cos(3\theta_L)=\sqrt{6}\ \mathrm{tr}\,\boldsymbol{n}^3;\boldsymbol{n}=\frac{\boldsymbol{r}-\boldsymbol{\alpha}}{[(\boldsymbol{r}-\boldsymbol{\alpha}):(\boldsymbol{r}-\boldsymbol{\alpha})]^{1/2}};\boldsymbol{r}=\frac{\boldsymbol{s}}{p'} \tag{5b}$$

where M_c and M_e are the critical stress ratios in compression and extension, respectively. According to Jiang and Pietruszczak (1988), the shape of Eq. (5) in the π plane might be concave when $M_e/M_c<7/9$, which is a shortcoming of Eq. (5) compared to other methods for introducing 3D strength such as the stress transformation method (Matsuoka and Sun, 2006). The potential function is a curved triangle as shown in Fig. 2, and both M_c and M_e are subtly considered in SANICLAY. Hence, the present solution can be seen as a more general solution to the cavity expansion problem than the exiting circular critical state line-based solutions, such as Chen and Abousleiman (2012), Sivasithamparam and Castro (2018).

The non-associated flow rule was employed in the SANICLAY model, which means the yield surface does not overlap the plastic potential surface. The tensorial form of the yield surface function in the general stress space is defined as

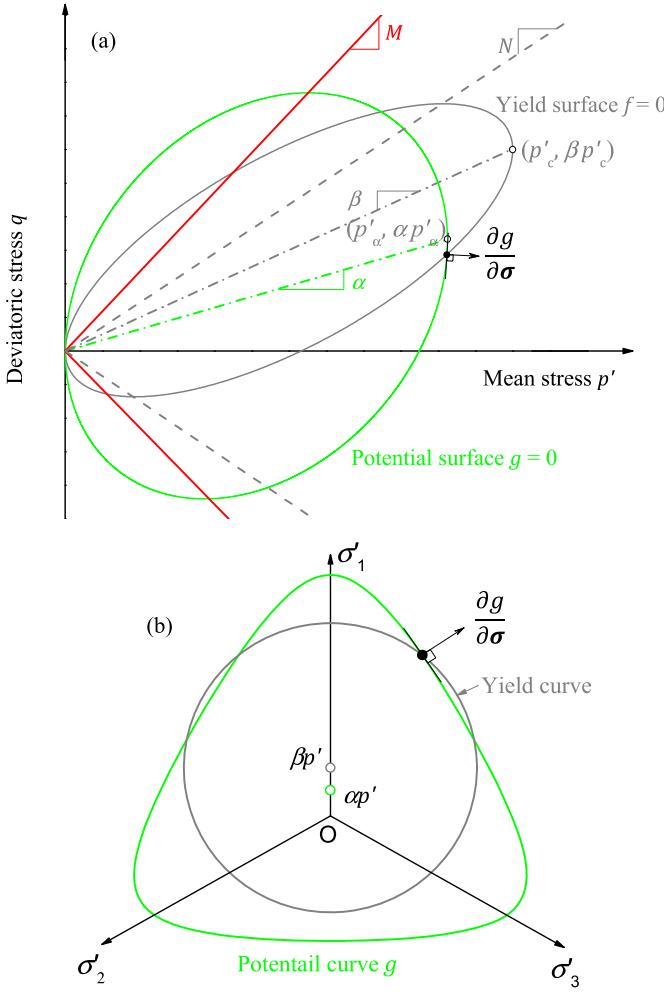

Fig. 2. Yield surface and plastic potential of the SANICLAY model in (a) $p'-q$ space and (b) π plane.

$$f = \frac{3}{2}(\boldsymbol{s} - p'\boldsymbol{\beta}) : (\boldsymbol{s} - p'\boldsymbol{\beta}) - \left(N^2 - \frac{3}{2}\boldsymbol{\beta} : \boldsymbol{\beta}\right)p'(p'_c - p') = 0 \tag{6}$$

where $\boldsymbol{\beta}$ is the rotational hardening variable tensor of yield surface; p'_c is the value of p' at $\eta = \beta_0$, where η is the stress ratio defined as q/p' and $\beta_0 = [(3/2)\boldsymbol{\beta}:\boldsymbol{\beta}]^{1/2}$, which represents the isotropic hardening variable; N is a soil constant that serves as the bound for $\boldsymbol{\beta}$ and is assumed independent on the Lode's angle. Again, the proposed solution with a non-associated flow rule can be regarded as a more general case than the existing associated constitutive model-based solutions, which is another predominant feature of this study.

Both yield surface and plastic potential surface are schematically illustrated in Fig. 2 in the p'-q space and the deviatoric plane, respectively. The critical stress state at failure is unnecessarily located at the peak of the yield surface in the p'-q space (Fig. 2a), contributing to the undrained softening after K_0-consolidation. The shape of yield function in the π plane is a circle, whereas the plastic potential surface is anisotropic owing to dependence on the Lode's angle. To describe the evolution of the internal variables serving as three hardening laws, the isotropic hardening parameter p'_c and the anisotropic rotational hardening parameter tensors $\boldsymbol{\alpha}$ (for plastic potential) and $\boldsymbol{\beta}$ (for yield surface) are defined in terms of their rate forms as

$$\dot{p}'_c = \langle L\rangle \overline{p}'_c = \langle L\rangle \frac{1+e_0}{\lambda-\kappa} p'_c \,\mathrm{tr}\left(\frac{\partial g}{\partial \boldsymbol{\sigma}}\right) \tag{7a}$$

$$\dot{\boldsymbol{\alpha}} = \langle L\rangle \overline{\boldsymbol{\alpha}} = \langle L\rangle \frac{v_0}{\lambda-\kappa} C\left(\frac{p'}{p'_c}\right)^2 \left|\mathrm{tr}\left(\frac{\partial g}{\partial \boldsymbol{\sigma}}\right)\right| \cdot \left[\frac{3}{2}(\boldsymbol{r} - x\boldsymbol{\alpha}) : (\boldsymbol{r} - x\boldsymbol{\alpha})\right]^{1/2} (\boldsymbol{\alpha}_b - \boldsymbol{\alpha}) \tag{7b}$$

$$\boldsymbol{\alpha}_b = \sqrt{2/3}M \frac{(\boldsymbol{r}/x) - \boldsymbol{\alpha}}{[(\boldsymbol{r}/x - \boldsymbol{\alpha}) : (\boldsymbol{r}/x - \boldsymbol{\alpha})]^{1/2}} \tag{7c}$$

$$\dot{\boldsymbol{\beta}} = \langle L\rangle \overline{\boldsymbol{\beta}} = \langle L\rangle \frac{1+e_0}{\lambda-\kappa} C\left(\frac{p'}{p'_c}\right)^2 \left|\mathrm{tr}\left(\frac{\partial g}{\partial \boldsymbol{\sigma}}\right)\right| \left[\frac{3}{2}(\boldsymbol{r} - \boldsymbol{\beta}) : (\boldsymbol{r} - \boldsymbol{\beta})\right]^{1/2} (\boldsymbol{\beta}_b - \boldsymbol{\beta}) \tag{7d}$$

$$\boldsymbol{\beta}_b = \sqrt{2/3}N \frac{\boldsymbol{r} - \boldsymbol{\beta}}{[(\boldsymbol{r} - \boldsymbol{\beta}) : (\boldsymbol{r} - \boldsymbol{\beta})]^{1/2}} \tag{7e}$$

where L is the loading index, which will be specified later from the plastic consistency condition; $\langle\ \rangle$ is the Macaulay bracket; e_0 is the initial void ratio, v_0 is the initial specific volume; λ and κ are the slopes of normal compression and swelling lines, respectively, in the $e - \ln p'$ space (e is the void ratio); C is a model constant, which represents the rate of evolution of anisotropy; the subscript 'b' is used for the bounding 'image' of the variable; x is another model parameter to define the attractor tensor $\boldsymbol{r}/x$ for $\boldsymbol{\alpha}$, indicating the saturation limit of anisotropy.

4. Undrained cavity expansion solution

4.1. Constitutive relationship in matrix form

In the classical plasticity theory, the incremental total strains in the plastic phase can be divided into elastic and plastic components, with superscripts 'e' and 'p', respectively. In terms of the cylindrical coordinates in this problem, the rates of the elastic strains can be represented by the effective stresses in the matrix form, following the small-strain assumption and the Hooke's law for isotropic mass:

$$\begin{bmatrix} \dot{\varepsilon}^e_r \\ \dot{\varepsilon}^e_\theta \\ \dot{\varepsilon}^e_z \end{bmatrix} = \frac{1}{E}\begin{bmatrix} 1 & -\mu & -\mu \\ -\mu & 1 & -\mu \\ -\mu & -\mu & 1 \end{bmatrix} \begin{bmatrix} \dot{\sigma}'_r \\ \dot{\sigma}'_\theta \\ \dot{\sigma}'_z \end{bmatrix} \tag{8}$$

where μ is the Poisson's ratio; E is the elastic modulus, which depends on the current effective mean stress p', specific volume v and basic soil parameters as

$$E = \frac{3(1-2\mu)vp'}{\kappa} \tag{9}$$

Based on the plastic flow rule (see Eq. (4)), the rate of the plastic strain tensor $\boldsymbol{\varepsilon}^p$ can be written as

$$\dot{\boldsymbol{\varepsilon}}^p = \langle L\rangle \frac{\partial g}{\partial \boldsymbol{\sigma}} \tag{10}$$

where

$$\frac{\partial g}{\partial \boldsymbol{\sigma}} = 3(\boldsymbol{s} - p'\boldsymbol{\alpha}) + \frac{1}{3}p'\left(M^2 - \eta^2\right)\boldsymbol{I} + \frac{\partial g}{\partial \theta_L}\frac{\partial \theta_L}{\partial \boldsymbol{\sigma}} \tag{11a}$$

$$\frac{\partial g}{\partial \theta_L} = 6M^2 p'(p'_\alpha - p')\frac{1 - M_e/M_c}{(1+M_e/M_c) - (1-M_e/M_c)\cos(3\theta_L)}\sin(3\theta_L) \tag{11b}$$

$$\frac{\partial \theta_L}{\partial \boldsymbol{\sigma}} = -\frac{\sqrt{6}}{\sin(3\theta_L)} \frac{\boldsymbol{n}^2 - \boldsymbol{n}\frac{\cos(3\theta_L)}{\sqrt{6}} - \frac{1}{3}\boldsymbol{I}\left[1 + \mathrm{tr}\left(\boldsymbol{n}^2\boldsymbol{\alpha}\right) - \frac{\cos(3\theta_L)}{\sqrt{6}}\mathrm{tr}\left(\boldsymbol{n}\boldsymbol{\alpha}\right)\right]}{[(\boldsymbol{s} - p'\boldsymbol{\alpha}) : (\boldsymbol{s} - p'\boldsymbol{\alpha})]^{1/2}} \tag{11c}$$

For determination of the loading index L, the plastic consistency condition needs to be fulfilled as follows:

$$\dot{f} = \frac{\partial f}{\partial \boldsymbol{\sigma}} : \dot{\boldsymbol{\sigma}} + \frac{\partial f}{\partial \boldsymbol{\beta}} : \dot{\boldsymbol{\beta}} + \frac{\partial f}{\partial p'_c}\dot{p}'_c = 0 \tag{12}$$

Substituting Eq. (7) into Eq. (12) yields the expression of loading index L:

$$L = \frac{1}{K_p}\frac{\partial f}{\partial \boldsymbol{\sigma}} : \dot{\boldsymbol{\sigma}} \tag{13a}$$

$$K_p = -\left(\frac{\partial f}{\partial p'_c}\overline{p}'_c + \frac{\partial f}{\partial \boldsymbol{\beta}} : \overline{\boldsymbol{\beta}}\right) \tag{13b}$$

where

$$\frac{\partial f}{\partial \boldsymbol{\sigma}} = 3(\boldsymbol{s} - p'\boldsymbol{\beta}) + \frac{1}{3}p'\left(N^2 - \eta^2\right)\boldsymbol{I} \tag{14a}$$

$$\frac{\partial f}{\partial p'_c} = -\left(N^2 - \frac{3}{2}\boldsymbol{\beta}:\boldsymbol{\beta}\right)p' \tag{14b}$$

$$\frac{\partial f}{\partial \boldsymbol{\beta}} = -3p'(\boldsymbol{s} - p'_c\boldsymbol{\beta}) \tag{14c}$$

The rates of the three plastic strain components can thus be re-written in the matrix form based on Eq. (10):

$$\begin{bmatrix} \dot{\varepsilon}_r^p \\ \dot{\varepsilon}_\theta^p \\ \dot{\varepsilon}_z^p \end{bmatrix} = \frac{1}{K_p}\begin{bmatrix} A_rB_r & A_rB_\theta & A_rB_z \\ A_\theta B_r & A_\theta B_\theta & A_\theta B_z \\ A_zB_r & A_zB_\theta & A_zB_z \end{bmatrix}\begin{bmatrix} \dot{\sigma}'_r \\ \dot{\sigma}'_\theta \\ \dot{\sigma}'_z \end{bmatrix} \tag{15}$$

where the matrix elements are given as

$$A_i = \frac{\partial g}{\partial \sigma'_i}(i = r,\theta,z) \tag{16a}$$

$$B_i = \frac{\partial f}{\partial \sigma'_i}(i = r,\theta,z) \tag{16b}$$

Combining the stress-strain relationships in Eqs. (8) and (15), the rates of stress components can be inversely expressed in terms of the incremental total strain components as follows:

$$\begin{bmatrix} \dot{\sigma}'_r \\ \dot{\sigma}'_\theta \\ \dot{\sigma}'_z \end{bmatrix} = \frac{1}{H}\begin{bmatrix} H_r & H_{r\theta} & H_{rz} \\ H_{\theta r} & H_\theta & H_{\theta z} \\ H_{zr} & H_{z\theta} & H_z \end{bmatrix}\begin{bmatrix} \dot{\varepsilon}_r \\ \dot{\varepsilon}_\theta \\ \dot{\varepsilon}_z \end{bmatrix} \tag{17}$$

where the matrix elements are given as

$$\begin{aligned} H = (\mu+1)\Big[K_p\left(1-\mu-2\mu^2\right) + E(1-\mu)(A_rB_r + A_\theta B_\theta + A_zB_z) \\ + E\mu(A_rB_\theta + A_\theta B_r + A_\theta A_z + A_zA_\theta + A_zB_r + A_rB_z)\Big] \end{aligned} \tag{18a}$$

$$\begin{aligned} H_i = E\Big[K_p\left(1-\mu^2\right) + E(A_jB_j + A_kB_k) + E\mu(A_jB_k + A_kB_j)\Big] \\ (i,j,k = r,\theta,z; i \neq j \neq k) \end{aligned} \tag{18b}$$

$$\begin{aligned} H_{ij} = E\Big[K_p\left(\mu+\mu^2\right) - EA_iB_j \\ + E\mu(A_kB_k - A_iB_k - A_kB_j)\Big](i,j,k = r,\theta,z; i \neq j \neq k) \end{aligned} \tag{18c}$$

4.2. Solution in the elastic region

At a K_0-consolidation condition before expansion, the initial stress relation gives $\sigma'_{h0} = K_0\sigma'_{v0}$. Considering the rotational hardening of the yield surface and plastic potential, the initial values of the dimensionless anisotropic variable tensors $\boldsymbol{\alpha}_0$ and $\boldsymbol{\beta}_0$ are related to the coefficient of lateral earth pressure at rest K_0 in terms of the cylindrical coordinates, as follows (Dafalias et al., 2006):

$$\boldsymbol{\alpha}_0 = \frac{\boldsymbol{r}_0}{x} = \frac{1}{x}\begin{bmatrix} \frac{K_0-1}{2K_0+1} & 0 & 0 \\ 0 & \frac{K_0-1}{2K_0+1} & 0 \\ 0 & 0 & \frac{2-2K_0}{2K_0+1} \end{bmatrix} \tag{19a}$$

$$\boldsymbol{\beta}_0 = \boldsymbol{r}_0 = \begin{bmatrix} \frac{K_0-1}{2K_0+1} & 0 & 0 \\ 0 & \frac{K_0-1}{2K_0+1} & 0 \\ 0 & 0 & \frac{2-2K_0}{2K_0+1} \end{bmatrix} \tag{19b}$$

The elastic region is located outside of the elastoplastic boundary with $r > r_p$ after cavity expansion. The elastic solution can then be expressed following the small-strain elasticity (Yu, 2020), as

$$\sigma'_r = \sigma'_{h0} + \left(\sigma'_{rp} - \sigma'_{h0}\right)\frac{r_p^2}{r^2} \tag{20a}$$

$$\sigma'_\theta = \sigma'_{h0} - \left(\sigma'_{rp} - \sigma'_{h0}\right)\frac{r_p^2}{r^2} \tag{20b}$$

$$\sigma'_z = \sigma'_{v0} \tag{20c}$$

$$U_r = \frac{1}{2G_0}\left(\sigma'_{rp} - \sigma'_{h0}\right)\frac{r_p^2}{r} \tag{20d}$$

where σ'_{rp} denotes the effective radial stress at the elastoplastic boundary, which will be determined in the following section; U_r is the radial displacement; G_0 is the shear modulus in the elastic region, taking $G = E/[2(1+\mu)]$ with Eq. (9). Note the excess pore pressure in the elastic region remains to be zero, owing to the unchanged mean stresses.

4.3. Solution in the plastic region

4.3.1. Conditions at elastic-plastic boundary

Soil states at the elastoplastic boundary are taken as the initial conditions for the solution within the plastic region. Combining the yield surface function, initial anisotropic tensor, and the stress state at the elastic-plastic boundary (Eqs. (6), (19b), and (20a)-(c)), the value of σ'_{rp} can be obtained as

$$\sigma'_{rp} = K_0\sigma'_{v0} + \frac{p'_0}{\sqrt{3}}\sqrt{\left(N^2 - \frac{3}{2}\boldsymbol{\beta}_0:\boldsymbol{\beta}_0\right)(OCR-1)} \tag{21}$$

where p'_0 is the in situ value of the effective mean stress (i.e. $p'_0 = (1+2K_0)\sigma'_{v0}/3$); OCR denotes the overconsolidation ratio and is defined as p'_{c0}/p'_0. Note that the value of OCR in this paper represents the isotropic overconsolidation ratio, in terms of the mean effective stress rather than the conventional vertical effective stress, following Mo and Yu (2017).

The ratio of the current position of one soil particle to its original position is introduced herein to indicate the relative deformation as a time variable, i.e. $\rho = r/r_0$. From the displacement distribution in the elastic region (see Eq. (20d)), the value of ρ at the elastic-plastic boundary is derived as

$$\rho_p = \frac{r_p}{r_{p0}} = \frac{1}{1-\frac{\sigma'_{rp}-K_0\sigma'_{v0}}{2G_0}} \tag{22}$$

The range of ρ within the plastic zone is given as

$$\rho_p \le \rho \le \rho_a = \frac{a}{a_0} \tag{23}$$

Considering the undrained condition with Eqs. (2) and (3), the current radial coordinate can be determined from ρ:

$$\frac{r}{a} = \sqrt{\frac{1-\left(\frac{a_0}{a}\right)^2}{1-\left(\frac{1}{\rho}\right)^2}} \tag{24}$$

4.3.2. Governing differential equations

In conjunction with the introduced definition of ρ and the undrained condition for a cylindrical scenario, the incremental strains can be re-written as

$$\dot{\varepsilon}_\theta = -\frac{\mathrm{D}\ln(\rho)}{\mathrm{D}\rho} = -\frac{1}{\rho} \tag{25a}$$

$$\dot{\varepsilon}_r = \dot{\varepsilon}_v - \dot{\varepsilon}_\theta - \dot{\varepsilon}_z = -\dot{\varepsilon}_\theta = \frac{1}{\rho} \tag{25b}$$

where D() is the material derivative along the particle motion path using the Lagrangian description.

Considering the undrained condition and the definition of ρ, the Eulerian derivative for every material particle at a specific moment can also be related to ρ as

$$\frac{\mathrm{d}()}{\mathrm{d}r} = \frac{\mathrm{D}()}{\mathrm{D}\rho}\frac{\mathrm{d}\rho}{\mathrm{d}r} = \left(\frac{1}{r_0} - \frac{r}{r_0^2}\frac{\mathrm{d}r_0}{\mathrm{d}r}\right)\frac{\mathrm{D}()}{\mathrm{D}\rho} = \frac{1}{r}\left[\rho - \rho^2\exp(\varepsilon_r)\right]\frac{\mathrm{D}()}{\mathrm{D}\rho} = \frac{\rho-\rho^3}{r}\frac{\mathrm{D}()}{\mathrm{D}\rho} \tag{26}$$

It should be noted that Eqs. (25) and (26) can be easily extended to their drained versions by taking the specific volume as an extra unknown. Then the proposed solving approach can be easily extended to the drained case, which shows the advantages of the utilized time variable ρ-based solving technique over the existing solutions.

By substituting the strain definitions of Eq. (25) into the constitutive matrix of Eq. (17), the components can be expressed as

$$\frac{\mathrm{D}\sigma'_r}{\mathrm{D}\rho} = \frac{H_r - H_{r\theta}}{\rho H} \tag{27a}$$

$$\frac{\mathrm{D}\sigma'_\theta}{\mathrm{D}\rho} = \frac{H_{\theta r} - H_\theta}{\rho H} \tag{27b}$$

$$\frac{\mathrm{D}\sigma'_z}{\mathrm{D}\rho} = \frac{H_{zr} - H_{z\theta}}{\rho H} \tag{27c}$$

It should be noted that both p'_c and p'_α are expressed by stresses, α and β according to Eqs. (4) and (6) during the updating of the constitutive matrix. Therefore, p'_α and p'_c are not involved in the constitutive matrix and not updated by integration.

Combining Eq. (1) with Eq. (26), the excess pore water pressure can be obtained as

$$\frac{Du}{D\rho} = -\frac{D\sigma'_r}{D\rho} - \frac{\sigma'_r - \sigma'_\theta}{\rho - \rho^3} = -\frac{H_r - H_{r\theta}}{\rho H} - \frac{\sigma'_r - \sigma'_\theta}{\rho - \rho^3} \tag{28}$$

It should be noted that Eqs. (27a-c) and (28) are first-order differential equations with respect to ρ. Substituting Eq. (25) back into Eqs. (7) and (13a), one can also express the rates of isotropic hardening parameter p'_c and anisotropic parameters α and β as functions regarding ρ, which are given in Appendix A. Therefore, the governing equations for the cavity expansion problem can now be simplified to a system of first-order differential equations, which can be solved by the Runge-Kutta method (Atkinson, 1989) via a computational software as shown in Fig. 3. The corresponding MATLAB source code can be found in Appendix A to facilitate the use of the presented solution, as well as a worked-out example. Since the cavity in the infinite medium expands in a self-similar way, all the soil particles experience the same stress path. Considering the relative deformation along with the position to the cavity wall, the stress and displacement distributions in both elastic and plastic regions are obtained, as well as their evolutions during the cavity expansion process.

5. Results and discussion

5.1. Validation against MCC solution

The proposed solution is firstly validated against the MCC solution proposed by Chen and Abousleiman (2012), excluding the anisotropy and non-associativity by setting $N = M_c = M_e$, $x = 1$ and $C = 0$. The soil parameters are set equivalent to those for the normally consolidated Boston Blue clay with $K_0 = 0.625$, after Chen and Abousleiman (2012), as detailed in Table 2.

The normalized distributions of stress components after a certain expansion with $a/a_0 = 2$ are compared in Fig. 4. The effective stresses (σ'_r, σ'_θ, σ'_z) and excess pore pressure (Δu) based on the recovered SANICLAY model are identical to those of the MCC solution, for both critical state and plastic regions, validating the developed formulation in the previous section. Additionally, comparing to the MCC solution, the advantages of the current solution lie on the rotation and distortion of both yield surface and plastic potential with respective evolution law considering K_0-consolidation and stress-induced anisotropy, as follows.

5.2. Influence of overconsolidation ratio

A parametric study is then conducted to present the results of cylindrical cavity expansion using the foregoing solution, examining the effects of overconsolidation ratio. All the SANICLAY model parameters are set as those from Dafalias et al. (2006) for the Lower Cromer Till (LCT) clay, and four tests with different *OCR* in the range of 1–10 are considered with identical initial effective mean stress ($p'_0 = 120$ kPa). The corresponding initial state parameters are summarized with details in Table 3.

The variations of the normalized cavity pressure (σ_a/p'_0) and excess pore pressure at the cavity wall ($\Delta u/p'_0$) during expansion from $a/a_0 = 1$ to $a/a_0 = 10$ are shown in Fig. 5, for tests of soil with various values of *OCR*. The cavity pressure increases rapidly at the initial expansion stage with $a/a_0 < 3$, which tends to approach an asymptotic limit pressure at a larger expansion period. The normalized cavity pressure appears to increase with *OCR*, and similar trends were also reported by Sivasithamparam and Castro

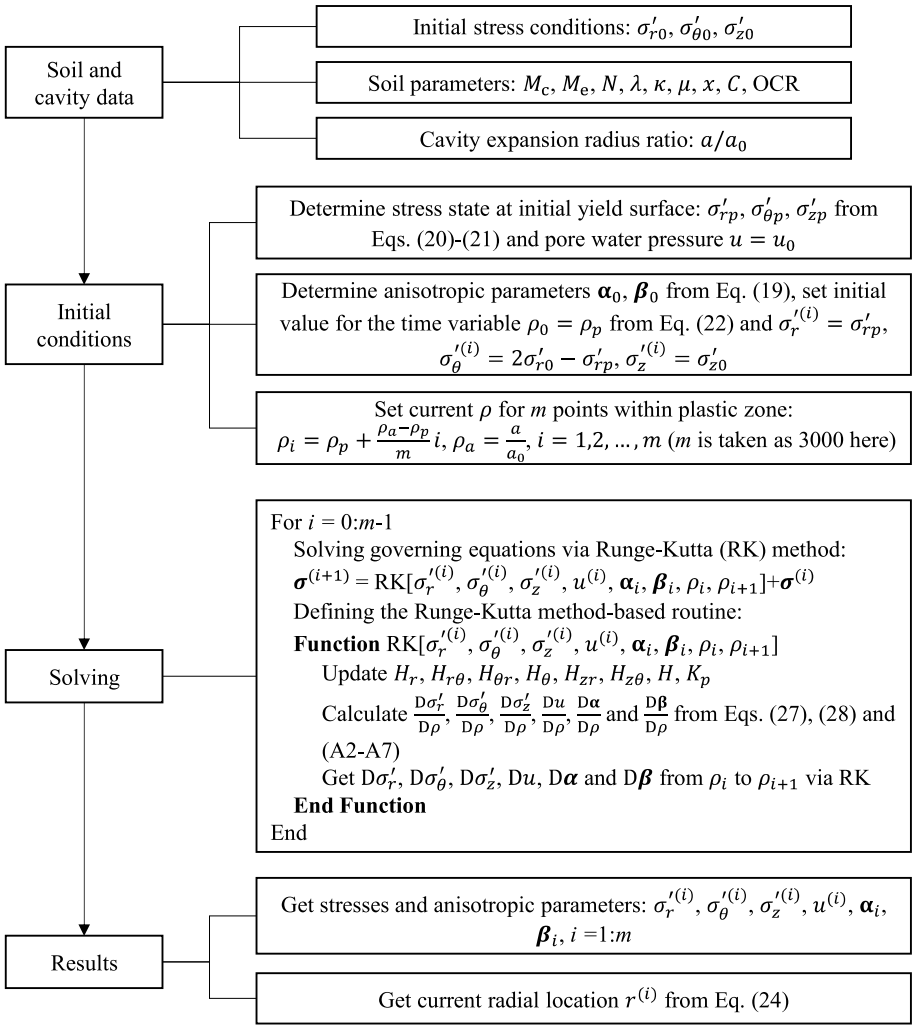

Fig. 3. Solving procedures for soil particle in plastic zone.

Table 2
Parameters of special case for comparison of present solution and MCC solution.

Soil model	M	M_c	M_e	λ	κ	μ	N	x	C
SANICLAY	–	1.2	1.2	0.15	0.03	0.278	1.2	1	0
MCC	1.2	–	–	0.15	0.03	0.278	–	–	–

Note: σ'_{h0} = 100 kPa, σ'_{v0} = 160 kPa, v_0 = 2.09, u_0 = 100 kPa, OCR = 1.

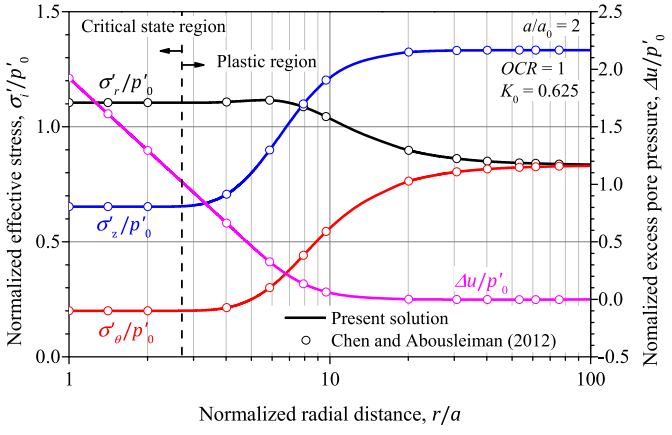

Fig. 4. Distributions of stress components of special case for comparison of present solution and MCC solution.

Table 3
Stress conditions and material properties of the LCT clay involved in parametric analysis. (Extended and revised from Chen and Abousleiman, 2012).

OCR	σ'_{h0} (kPa)	σ'_{v0} (kPa)	u_0 (kPa)	K_0	p'_0 (kPa)	q_0 (kPa)	v_0	G_0 (kPa)
1	100	160	100	0.625	120	60	2.04	20358
3	120	120	100	1	120	0	1.98	19765
5	130	100	100	1.3	120	30	1.95	19489
10	144	72	100	2	120	72	1.91	19114

Note: M_c = 1.18, M_e = 0.86, λ = 0.063, κ = 0.009, μ = 0.2, N = 0.91, x = 1.56, C = 16.

(2018). The excess pore pressure at the cavity wall, as depicted in Fig. 5b, shows generally a gradual increase at $a/a_0 < 4$, and also approaches the limiting value at notable expansion. The soil with a larger value of OCR is found to have a higher limiting value of normalized excess pore pressure. However, slight negative excess pore pressure appears during the very early expansion with $a/a_0 <$ 1.1 for heavily overconsolidated soil with OCR = 10, which is consistent with those in Chen and Abousleiman (2012) and Li et al. (2016b).

The distributions of effective stresses and excess pore pressure at an expansion instant of a/a_0 = 2 are provided in Fig. 6, for all cases with various values of OCR in the range 1–10. All stress components are normalized by the initial effective mean stress p'_0, and the radial distance of soil element to the cavity center r is

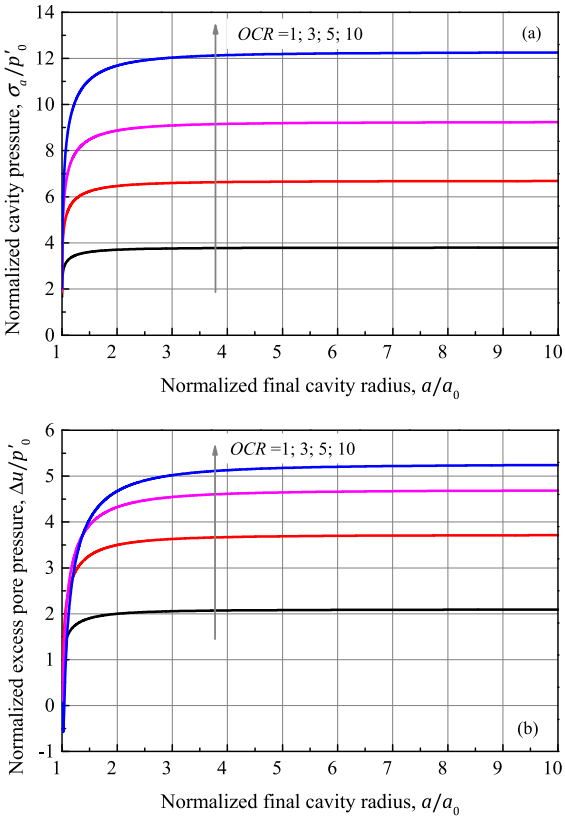

Fig. 5. Variations of (a) normalized cavity pressure and (b) normalized excess pore pressure at cavity wall during expansion in soil with different values of *OCR*.

normalized by the current cavity radius a. For normally consolidated clay (Fig. 6a), any degree of expansion causes the plastic yielding, leading to an infinite plastic region. For the isotropically consolidated clay with $K_0 = 1$ in Fig. 6b, the effective stresses converge to an identical constant at far field of the elastic region for undisturbed soil element after expansion. Stress changes at the elastoplastic boundary are shown unsmooth, especially for the circumferential stress. The radial stress in the elastic region decreases with radial distance, whereas the mean stress, vertical stress and pore pressure remain constants during the elastic stage, as reflected in Eq. (20). The effective stresses in the vicinity of the cavity wall are uniform within the critical state regions, while the excess pore pressure decreases almost linearly with the logarithmic scale of the radial distance and the size of the critical state region decreases with the value of *OCR*. The size of the plastic region is also found to decrease with the overconsolidation ratio, and negative excess pore pressure is shown in the distribution curve for heavily overconsolidated clay (Fig. 6d). Note that the effective vertical stress is not always the intermediate principal stress in the critical state region, for example as shown in Fig. 6d, which was also reported by Chen and Liu (2019) but is against that of Chen and Abousleiman (2012), where the ultimate vertical stress equalled to the average of radial and circumferential stresses.

Correspondingly, Fig. 7 presents the distributions of anisotropic parameters (α and β) after undrained expansion of $a/a_0 = 2$ for all tests with various values of *OCR*. All parameters in both critical state and elastic regions remain constant, while the monotonical transitions appear in the plastic regions, indicating the rotation and distortion of yield surface and plastic potential with plastic yielding. It should be noted that the magnitudes of

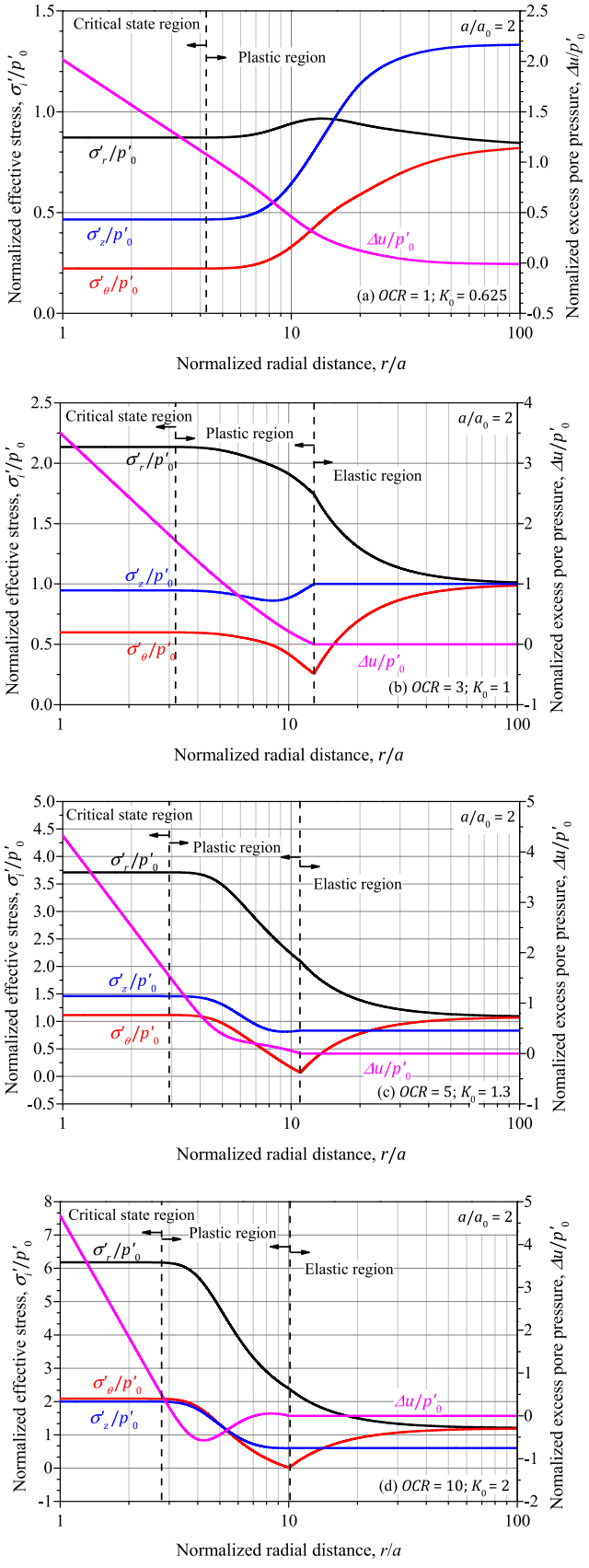

Fig. 6. Distributions of normalized stresses and excess pore pressure after undrained expansion of $a/a_0 = 2$. (a) $OCR = 1$, $K_0 = 0.625$; (b) $OCR = 3$, $K_0 = 1$; (c) $OCR = 5$, $K_0 = 1.3$; (d) $OCR = 10$, $K_0 = 2$.

radial and circumferential parameters are identical at the elastic stage (i.e. $\alpha_{r0} = \alpha_{\theta 0}$ and $\beta_{r0} = \beta_{\theta 0}$), due to the initial vertical cross anisotropy. They start to deviate from each other at the elastoplastic boundary, and the amounts of changes of parameters represent the degree of induced anisotropy. Following the definitions of Eq. (19), the anisotropic parameters converge to zeros in the elastic region for isotropically consolidated clay (Fig. 7b). The radial parameters (α_r and β_r) tend to increase with expansion while the circumferential parameters show opposite trends for all tests with the *OCR* in range of 1–10. It is interesting to find that the vertical parameters (α_z and β_z) decrease with expansion for normally consolidated and lightly overconsolidated soils, whereas they increase slightly with expansion for heavily overconsolidated soil (Fig. 7d). However, the restrictive relations of $\alpha_r + \alpha_\theta + \alpha_z = 0$ and $\beta_r + \beta_\theta + \beta_z = 0$ hold true during the whole stages of cavity expansion, as also reported by Chen and Liu (2019). This is because the following equations maintain zero throughout the expansion process:

$$\dot{\alpha}_r + \dot{\alpha}_\theta + \dot{\alpha}_z = \mathrm{tr}(\dot{\boldsymbol{\alpha}}) \propto \mathrm{tr}(\boldsymbol{\alpha}_\mathrm{b} - \boldsymbol{\alpha}) = 0 \tag{29a}$$

$$\dot{\beta}_r + \dot{\beta}_\theta + \dot{\beta}_z = \mathrm{tr}(\dot{\boldsymbol{\beta}}) \propto \mathrm{tr}(\boldsymbol{\beta}_\mathrm{b} - \boldsymbol{\beta}) = 0 \tag{29b}$$

the initial cross-anisotropy and depends on the magnitude of *OCR* value. The shape of yield surface is a circle in the π plane, while the plastic potential function gives a smoothed-triangular surface owing to the non-associated flow rule and the 3D definition of critical stress ratio in Eq. (5). The shape of the potential function is concave as the ratio of M_e to M_c in this study is only 0.729. This value is less than the convexity criterion value 7/9 for Eq. (5) according to the research on the convexness of Eq. (5) by Jiang and Pietruszczak (1988). It should be noted that the initial yield surface returns to a single point 'O' for normally consolidated soil (Fig. 9a). The evolutions of yield and plastic potential surfaces are clearly shown, along with the ESPs during undrained expansion. Note that the horizontal elastic trajectory in Fig. 9b represents the unchanged vertical stress during the elastic expansion, and the final critical states are unnecessarily located at a specific Lode's angle ($\theta_\mathrm{L} = \pi/2$), as reported by Sivasithamparam and Castro (2018, 2020). It should be noted that the elastic volumetric strain rate plastic $\dot{\varepsilon}_\mathrm{v}^\mathrm{e}$ is null at the critical state. Then considering the undrained condition, the volumetric strain rate $\dot{\varepsilon}_\mathrm{v}^\mathrm{p}$ should also vanish (i.e. tr $(\partial g/\partial \boldsymbol{\sigma}) = 0$) at the critical state, thus no unique relation between $\boldsymbol{\alpha}$ and $\boldsymbol{r}$ can be found as indicated by Eq. (7b). Following Chen et al. (2019), combing Eq. (27a-c) gives

$$\begin{aligned}\frac{\mathrm{D}(2\sigma'_z - \sigma'_r - \sigma'_\theta)}{\mathrm{D}\rho} &= \frac{E(1-2\mu)(B_r - B_\theta)(A_r + A_\theta - 2A_z)}{\rho H} \\ &= \frac{3E(1-2\mu)(B_r - B_\theta)}{\rho H}\left[(\sigma'_r + \sigma'_\theta - 2\sigma'_z) - p'(\alpha_r + \alpha_\theta - 2\alpha_z) + \frac{1}{3}\frac{\partial g}{\partial \theta_\mathrm{L}}\left(\frac{\partial \theta_\mathrm{L}}{\partial \sigma'_r} + \frac{\partial \theta_\mathrm{L}}{\partial \sigma'_\theta} - 2\frac{\partial \theta_\mathrm{L}}{\partial \sigma'_z}\right)\right]\end{aligned} \tag{30}$$

The effective stress paths (ESP) of cavity expansion in both normally consolidated and heavily overconsolidated soils are depicted in the $p' - q$ plane with normalization of the initial effective mean stress (Fig. 8). The initial stress states, represented by the notation 'O' in the figure, are located at the K_0-line ($q/p' = 3|1 - K_0|/(1 + 2K_0)$) for K_0-consolidated soil, and both initial yield and plastic potential surfaces plotted in dash lines intersect at point 'O'. As for critical-state theory, the hardening/softening behaviour of soil is associated with stress ratio $\eta\,(q/p')$ rather than shear stress q according to Wood (1990). The expansion for normally consolidated soil (Fig. 8a) causes immediately plastic yielding with rotation and distortion of yield and plastic potential surfaces. The ESP describes the evolutions of effective stresses during undrained expansion, and clearly reflects the hardening behaviour (increase of stress ratio η) with the loading history of cavity expansion. The stress state approaches to the final point ('F' in the figures) at the critical state line (CSL). It should be noted that the ESP does not intersect with the final potential surface because the extension of the potential surface from p' axis is much smaller during loading than its final state (Fig. 8b). For heavily overconsolidated soil in Fig. 8b, the vertical elastic trajectory is firstly shown to reach its initial yield condition at the 'dry' side of the CSL ($q/p' > M$). Plastic softening behaviour (decrease of stress ratio η) is then observed during the plastic stage, and the stress path eventually terminates at a critical state as well.

In terms of the anisotropic stress condition in conjunction with the distortion and rotation of yield and plastic potential surfaces, the ESPs are depicted in the deviatoric (π) plane (Fig. 9), for both normally consolidated and heavily overconsolidated soils. The initial 'O' points along the σ'_z axis indicate the K_0 stress anisotropy, and the axisymmetric location of the initial plastic potential implies

Due to the existence of $\partial g/3\partial\theta_\mathrm{L}(\partial\theta_\mathrm{L}/\partial\sigma'_r + \partial\theta_\mathrm{L}/\partial\sigma'_\theta - 2\partial\theta_\mathrm{L}/\partial\sigma'_z)$ and the lack of determined relation between $\boldsymbol{\alpha}$ and $\boldsymbol{r}$, Eq. (30) does not guarantee $\sigma'_z = (\sigma'_r + \sigma'_\theta)/2$ and $\alpha_z = (\alpha_r + \alpha_\theta)/2$ at the critical state and this is the reason that the ESPs would not always terminate at $\theta_\mathrm{L} = \pi/2$.

5.3. Effects of model constants

The test of normally consolidated clay in Table 3 ($OCR = 1$) is taken as a reference in this section, for investigating effects of the three new model constants of SANICLAY (i.e. N, x and C), compared with the MCC model. The parameter 'N' was used to define the shape of the yield surface in Eq. (6) that introduces the non-associativity compared with the plastic potential defined by Eq. (4) with anisotropic value of M. A restrained condition was also noted by Dafalias et al. (2006) with $M_\mathrm{e} \leq N < M_\mathrm{c}$ for predictions of softening behaviour following K_0-consolidation only in the compression scenarios. The effects of N value between 0.91 and 1.1 are shown in Fig. 10, with respect to the changes of the stress distributions and the stress paths. The increase of N results in the rise of all effective stresses (σ'_r, σ'_θ and σ'_z) in both plastic and critical state regions, whereas the magnitude of the increase of σ'_r is more notable than the others. However, the excess pore pressure in the plastic region is reversely smaller for tests with higher value of N. It is clear to notice the effects on the stress paths on the normalized $p' - q$ plane (Fig. 10b), while all tests seem to fall on an identical critical state line (CSL) after expansion. The stress path rises with N value, indicating the increases of mean and deviatoric stresses during expansion. The stress paths in the π plane are depicted in Fig. 10c, and the critical state surface at failure ($\mathrm{CSL_f}$) expands with N again, showing plastic hardening. Note that the shape of plastic

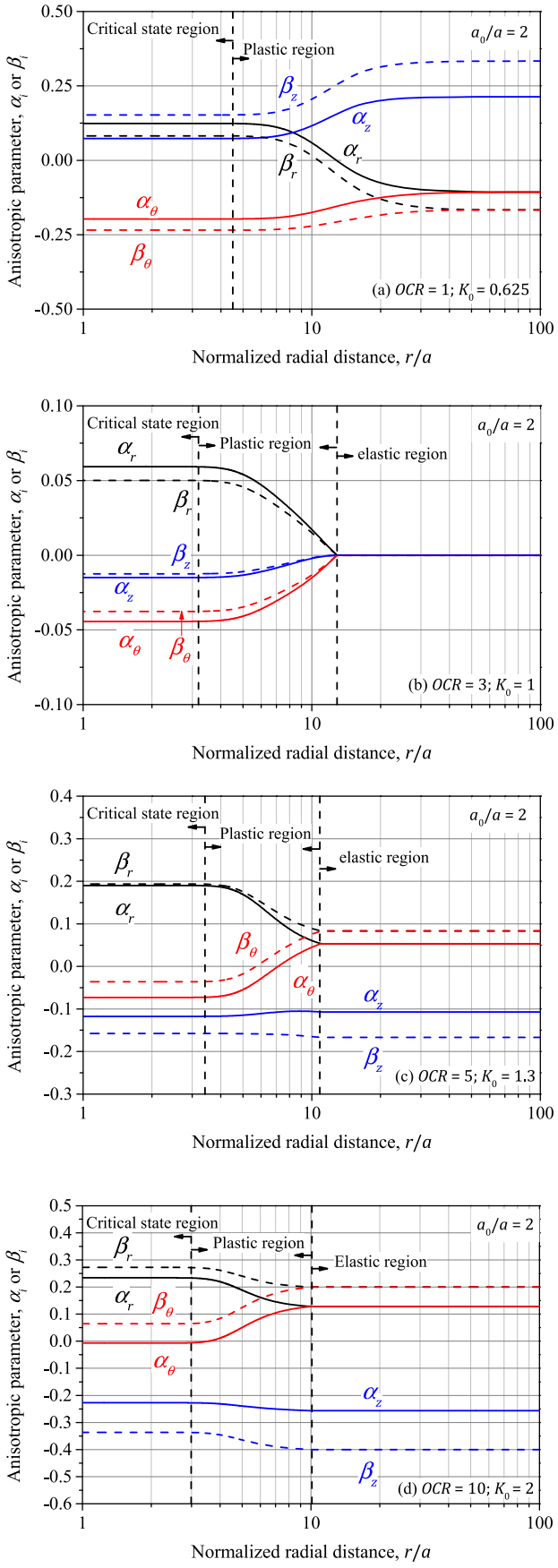

Fig. 7. Distributions of anisotropy parameters after undrained expansion of $a/a_0 = 2$. (a) $OCR = 1$, $K_0 = 0.625$; (b) $OCR = 3$, $K_0 = 1$; (c) $OCR = 5$, $K_0 = 1.3$; (d) $OCR = 10$, $K_0 = 2$.

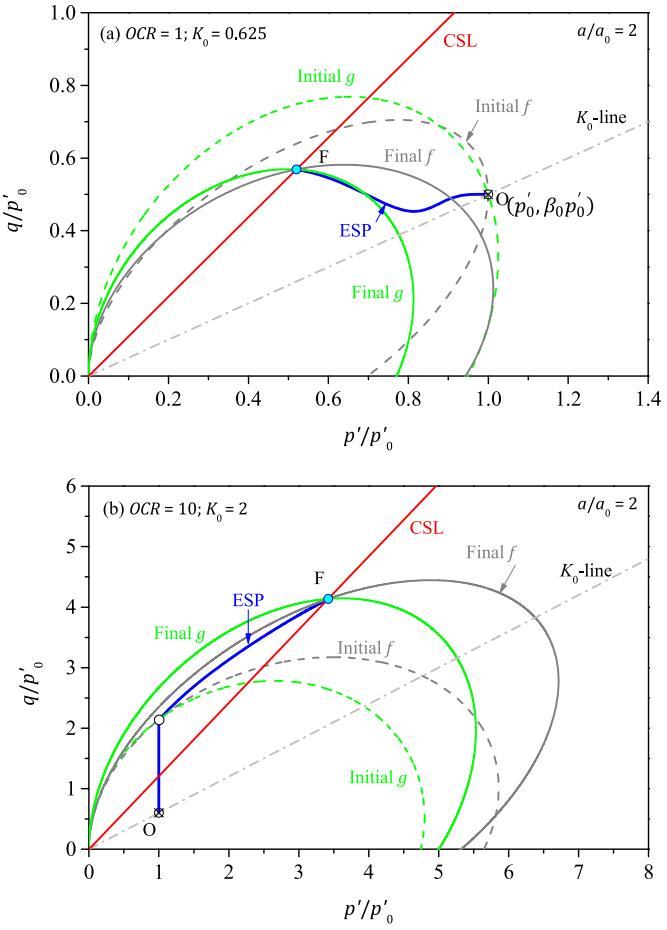

Fig. 8. Effective stress paths in $p' - q$ plane during undrained expansion of $a/a_0 = 2$. (a) $OCR = 1$, $K_0 = 0.625$; (b) $OCR = 10$, $K_0 = 2$.

potential and the critical state surface are analogues, owing to the identical Lode's angle dependent critical stress ratio. Moreover, the final states after cavity expansion are located at the same Lode's angle, giving the identical CSL in Fig. 10b, since the rotational hardening is not affected by the value of N.

The parameter 'x' was introduced to define the 'attractor' tensor, for $\boldsymbol{\alpha}$, that accounts for the anisotropy in the plastic potential. In Fig. 11, it shows the influences of x on the stress distributions and the stress paths of cavity expansion. When x varies between 1 and 2, the influence on the distributions of effective radial and circumferential stresses and the excess pore pressure is relatively limited, while the decrease of effective vertical stress with the magnitude of x is more distinct in the plastic and critical state regions. The stress paths in the $p' - q$ plane (Fig. 11b) show that both effective mean and deviatoric stresses at failure decrease marginally with x, whereas the stress ratio at the critical state appears to increase slightly with x. It is worth noting that the CSL differs from each other, despite the identical stress ratios at the critical state in compression and extension (i.e. $M_c = 1.18$, $M_e = 0.86$). It is attributed to the different rotational hardening of the plastic potential with changes of x, and the critical stress ratio M depends on Lode's angle that can be observed from the π plane (Fig. 11c). The ultimate Lode's angle decreases nonlinearly with x, and the size of the critical state surface at failure in the π plane reduces with x, indicating less plastic hardening.

The parameter 'C' was adopted in Eqs. (7b) and (7d) for determination of the rates of evolutions for the anisotropy variables (i.e. $\dot{\boldsymbol{\alpha}}$ and $\dot{\boldsymbol{\beta}}$), and Dafalias et al. (2006) suggested that the magnitude of

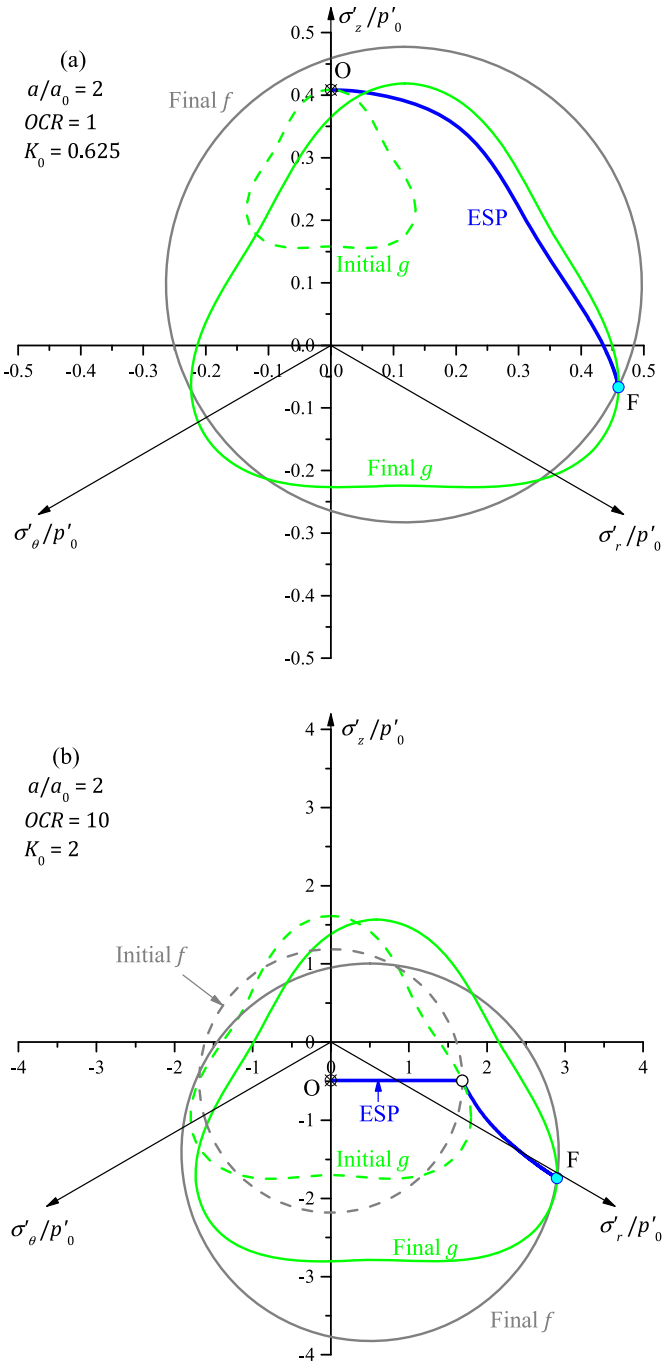

Fig. 9. Effective stress paths in π plane during undrained expansion of $a/a_0 = 2$. (a) $OCR = 1$, $K_0 = 0.625$; (b) $OCR = 10$, $K_0 = 2$.

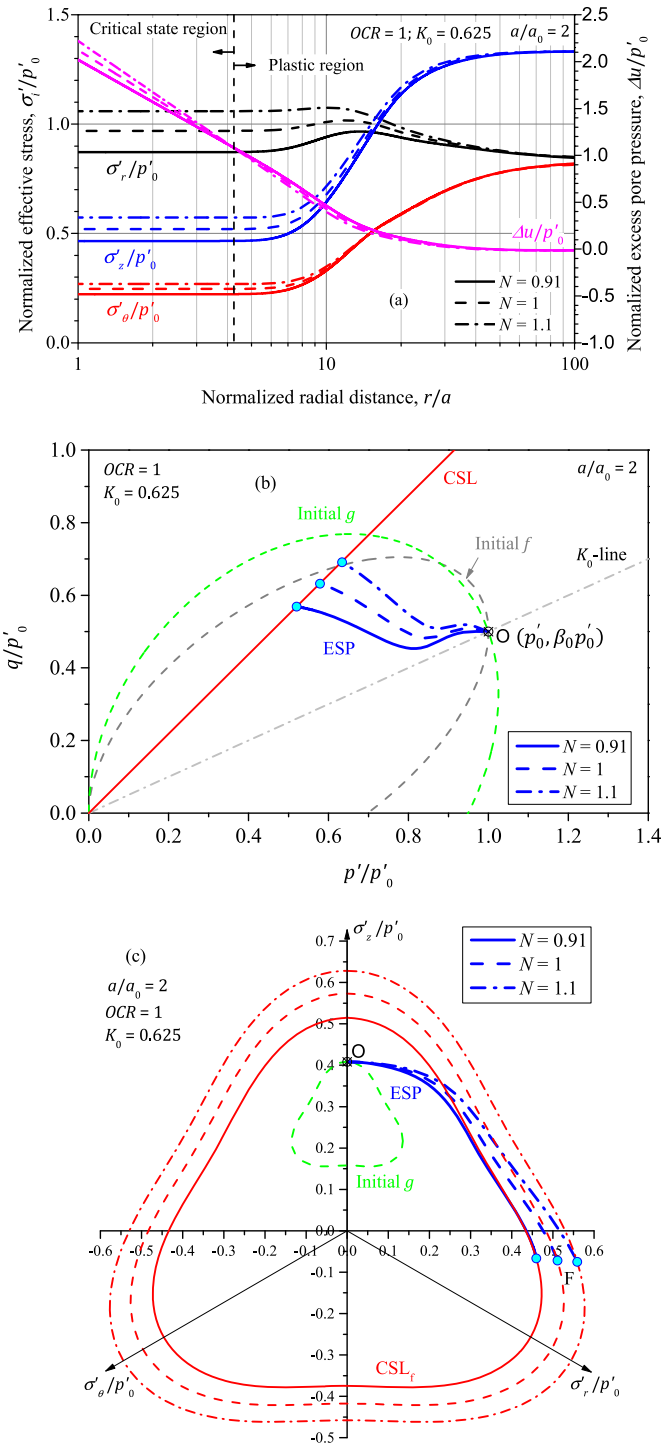

Fig. 10. Effects of N on (a) stress distributions after cavity expansion; (b) stress paths in $p' - q$ plane; (c) stress paths and critical state surfaces in π plane.

C is usually between 3 and 20 for various clays. The effects of C are presented in Fig. 12, with the variation of C between 11 and 21. Higher effective stresses are noticed for tests with larger C value, and the excess pore pressure in the critical state region increases slightly with C. Fig. 12b shows that the stress paths in the $p' - q$ plane for cavity expansion rise with C value, and the stress ratios at failure are quite close with a tiny growth against C. It is also illustrated in Fig. 12c with the stress paths in the π plane, providing larger critical state surfaces and lower Lode's angles at failure for tests with higher C value.

It is noticed that the model constants have significant effects on the stress distributions and paths during the undrained cavity expansion, and the uniqueness of the critical state is affected by the anisotropy and the evolution laws. The developed solution can provide more possibilities for accurate predictions and back-calculations, with considerations of K_0-consolidation and the stress-induced anisotropy. The proposed solution in SANICLAY is rigorously formulated, and the governing differential equations are

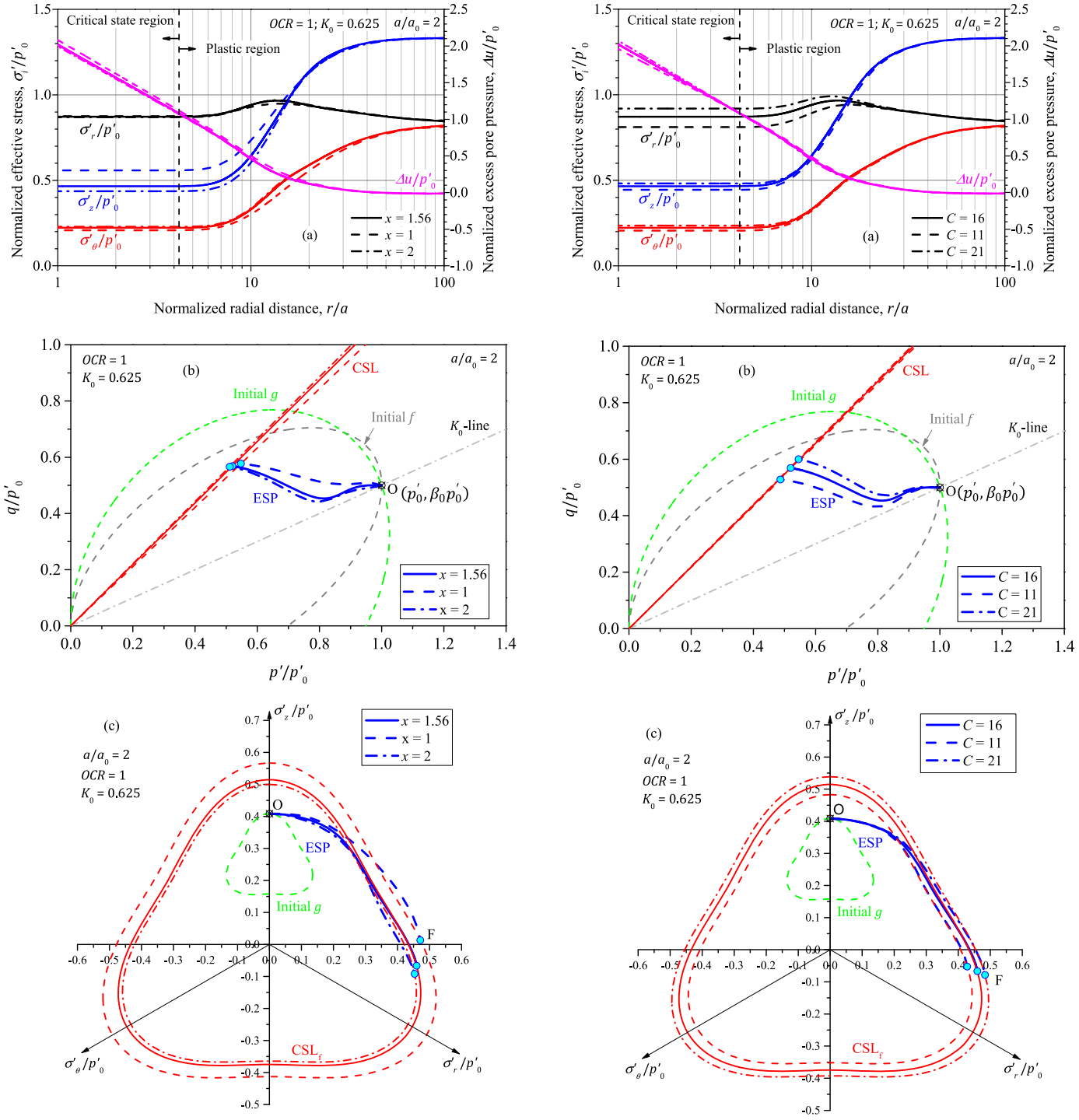

Fig. 11. Effects of x on (a) stress distributions after cavity expansion; (b) stress paths in $p' - q$ plane; (c) stress paths and critical state surfaces in π plane.

Fig. 12. Effects of C on (a) stress distributions after cavity expansion; (b) stress paths in $p' - q$ plane; (c) stress paths and critical state surfaces in π plane.

numerically solved for the stress and strain fields around the expanded cavities. Further considering the rate-dependent behaviour and destructuration upon loading, the presented framework is thus suitable for extensions using other SANICLAY based soil models (e.g. Taiebat et al., 2010; Seidalinov and Taiebat, 2014; Rezania et al., 2016). The current solution without introducing any assumptions, along with the provided source code, can also potentially serve as a benchmark for the extended analytical solutions and for the simplified numerical simulations of cavity expansion problems.

6. Conclusions

A rigorous semi-analytical solution of undrained cylindrical cavity expansion in the SANICLAY model is proposed in this paper, considering the K_0-consolidation and the stress-induced

anisotropy. The corresponding MATLAB source code is attached to facilitate the use of the solution and to serve as a benchmark for validations and extensions. Comparing to the MCC model, three model constants were introduced to include the 3D strength, non-associativity, rotational and distortional hardening, and the evolution laws in the multiaxial stress space. By utilizing a time variable ρ, both the position derivative and particle derivative can be converted to the same framework, thus the time variable-based solving technique can be used for both undrained and drained cavity problems. The exact derivation yields to the governing first-order differential equations, and the stress and strain distributions around the cavity after a certain expansion can be obtained effectively for all elastic, plastic and critical state regions, by adopting the Runge-Kutta method. The developed solution is firstly validated against the well accepted MCC solution, by setting constants for model recovering. Four tests in Lower Cromer Till clay with various overconsolidation ratio or alternatively the at-rest earth pressure coefficient K_0 are then conducted to examine the influences on the cavity pressure curves, stress distributions, evolutions of anisotropic parameters, and stress paths. The 3D evolutions of yield surface and plastic potential during cavity expansion in K_0-consolidated clays are accurately captured by the solution in a non-associated anisotropic model without introducing assumptions and complexities. The effects of new model constants are also investigated, indicating the abilities with various stress paths, critical state surfaces and Lode's angles at failure. The proposed procedure is also capable for further extensions, and the solution is potentially useful for verifying numerical results and for back-analyses of geotechnical problems, including pressuremeter tests and pile installation.

Declaration of competing interest

The authors declare that they have no known competing financial interests or personal relationships that could have appeared to influence the work reported in this paper.

Acknowledgments

We acknowledge the funding support from National Natural Science Foundation of China (Grant Nos. 51908546 and 52178374) and China Postdoctoral Science Foundation (Grant No. 2020T130699).

Appendix A. Supplementary data

Supplementary data to this article can be found online at https://doi.org/10.1016/j.jrmge.2021.10.016.

References

Atkinson, K.A., 1989. An Introduction to Numerical Analysis. John Wiley & Sons, New York, USA.
Bishop, R.F., Hill, R., Mott, N.F., 1945. Theory of identation and hardness tests. Proc. Phys. Soc. 57, 147–159.
Cao, L.F., Teh, C.I., Chang, M.F., 2001. Undrained cavity expansion in modified Cam clay I: theoretical analysis. Geotechnique 51, 323–334.
Carter, J.P., Booker, J.R., Yeung, S.K., 1986. Cavity expansion in cohesive frictional soils. Geotechnique 36, 349–353.
Chadwick, P., 1959. The quasi-static expansion of spherical cavity in metals and ideal soils. Quart. J. Mech. Appl. Math. 12, 52–71.
Chen, H.H., Li, L., Li, J.P., Sun, D.A., 2020. Elastoplastic solution to drained expansion of a cylindrical cavity in anisotropic critical-state soils. J. Eng. Mech. 146, 04020036.
Chen, H.H., Li, L., Li, J.P., Wang, H., 2019. Stress transform method to undrained and drained expansion of a cylindrical cavity in anisotropic modified cam-clay soils. Comput. Geotech. 106, 128–142.
Chen, H.H., Zhu, H.H., Zhang, L.Y., 2021. Analytical solution for Deep circular tunnels in Rock with consideration of disturbed zone, 3D strength and large strain. Rock Mech. Rock Eng. 54, 1391–1410.
Chen, S.L., Abousleiman, Y.N., 2012. Exact undrained elastoplastic solution for cylindrical cavity expansion in modified Cam clay soil. Geotechnique 62, 447–456.
Chen, S.L., Abousleiman, Y.N., 2013. Exact drained solution for cylindrical cavity expansion in modified Cam Clay soil. Geotechnique 63, 510–517.
Chen, S.L., Abousleiman, Y.N., 2018. Cavity expansion in strain hardening frictional soils under drained condition. Int. J. Numer. Anal. Methods GeoMech. 42, 132–142.
Chen, S.L., Liu, K., 2019. Undrained cylindrical cavity expansion in anisotropic critical state soils. Geotechnique 69, 189–202.
Chen, S.L., Liu, K., Castro, J., Sivasithamparam, N., 2019. Discussion on 'Undrained cylindrical cavity expansion in anisotropic critical state soils. Geotechnique 69, 1026–1028.
Dafalias, Y.F., 1986. An anisotropic critical state soil plasticity model. Mech. Res. Commun. 13, 341–347.
Dafalias, Y.F., 1987. An anisotropic critical state clay plasticity model. In: Desai, C.S., Krempl, E., Kiousis, P.D., Kundu, T. (Eds.), Proceedings of the Constitutive Laws for Engineering Materials: Theory and Applications, pp. 513–521. Tucson, Arizona, USA.
Dafalias, Y.F., Manzari, M.T., Papadimitriou, A.G., 2006. SANICLAY: simple anisotropic clay plasticity model. Int. J. Numer. Anal. Methods GeoMech. 30, 1231–1257.
Dafalias, Y.F., Taiebat, M., 2013. Anatomy of rotational hardening in clay plasticity. Geotechnique 63, 1406–1418.
Einav, I., 2007. Breakage mechanics - Part I: theory. J. Mech. Phys. Solid. 55 (6), 1274–1297.
Ghaboussi, J., Momen, H., 1984. Plasticity model for inherently anisotropic behavior of sands. Int. J. Numer. Anal. Methods GeoMech. 8, 1–16.
Hill, R., 1950. The Mathematical Theory of Plasticity. Oxford University Press, London, UK.
Jiang, J., Ling, H.I., Kaliakin, V.N., 2012. An associative and non-associative anisotropic bounding surface model for clay. J. Appl. Mech. 79, 031010.
Jiang, J., Pietruszczak, S., 1988. Convexity of yield loci for pressure sensitive materials. Comput. Geotech. 5, 51–63.
Karstunen, M., Krenn, H., Wheeler, S.J., Koskinen, M., Zentar, R., 2005. Effect of anisotropy and destructuration on the behaviour of Murro test embankment. Int. J. GeoMech. 5, 87–97.
Kelln, C., Sharma, J., Hughes, D., Graham, J., 2008. An improved elastic-viscoplastic soil model. Can. Geotech. J. 45 (10), 1356–1376.
Laloui, L., François, B., 2009. ACMEG-T: soil thermoplasticity model. J. Eng. Mech. 135 (9), 932–944.
Li, J.P., Gong, W.B., Li, L., Liu, F., 2017. Drained elastoplastic solution for cylindrical cavity expansion in K_0-consolidated anisotropic soil. J. Eng. Mech. 143, 04017133.
Li, L., Li, J., Sun, D., 2016a. Anisotropically elasto-plastic solution to undrained cylindrical cavity expansion in K_0-consolidated clay. Comput. Geotech. 73, 83–90.
Li, J., Li, L., Sun, D., Rao, P., 2016b. Analysis of undrained cylindrical cavity expansion considering three-dimensional strength of soils. Int. J. GeoMech. 16, 04016017.
Liu, H.L., Zhou, H., Wang, Z.L., Li, X., 2021. Theoretical solution for cavity expansion in crushable soil. Int. J. GeoMech. 21 (7), 04021098.
Liu, K., Chen, S.L., 2018. Analysis of cylindrical cavity expansion in anisotropic critical state soils under drained conditions. Can. Geotech. J. 56.
Matsuoka, H., Sun, D.A., 2006. The SMP Concept-Based 3D Constitutive Models for Geomaterials. CRC Press, Florida, USA.
Mayne, P.W., 1985. Stress anisotropy effects on clay strength. J. Geotech. Eng. 111, 356–366.
Mo, P.Q., Yu, H.S., 2017. Undrained cavity expansion analysis with a unified state parameter model for clay and sand. Geotechnique 67, 503–515.
Mo, P.Q., Yu, H.S., 2018. Drained cavity expansion analysis with a unified state parameter model for clay and sand. Can. Geotech. J. 67, 1–13.
Naggar, H.E., Naggar, M.H., 2012. Expansion of cavities embedded in cohesionless elastoplastic half-space and subjected to anisotropic stress field. Geotech. Geol. Eng. 30, 1183–1195.
Nakase, A., Kamei, T., 1983. Undrained shear strength anisotropy of normally consolidated cohesive soils. Soils Found. 23, 91–101.
Rezania, M., Taiebat, M., Poletti, E., 2016. A viscoplastic saniclay model for natural soft soils. Comput. Geotech. 73, 128–141.
Seidalinov, G., Taiebat, M., 2014. Bounding surface SANICLAY plasticity model for cyclic clay behavior. Int. J. Numer. Anal. Methods GeoMech. 38, 702–724.
Sekiguchi, H., Ohta, H., 1977. Induced anisotropy and time dependency in clays. In: Constitutive Equations of Soils. Proceedings of the 9th International Conference on Soil Mechanics and Foundation Engineering, pp. 306–315. Tokyo, Japan.
Sivasithamparam, N., Castro, J., 2018. Undrained expansion of a cylindrical cavity in clays with fabric anisotropy: theoretical solution. Acta Geotech. 13, 729–746.
Sivasithamparam, N., Castro, J., 2020. Undrained cylindrical cavity expansion in clays with fabric anisotropy and structure: theoretical solution. Comput. Geotech. 120, 103386.
Taiebat, M., Dafalias, Y.F., Peek, R., 2010. A destructuration theory and its application to SANICLAY model. Int. J. Numer. Anal. Methods GeoMech. 34, 1009–1040.
Vesic, A.C., 1972. Expansion of cavities in infinite soil mass. J. Soil Mech. Found Div. 98, 265–290.
Wang, L., Shen, K., Ye, S., 2008. Undrained shear strength of K_0 consolidated soft soils. Int. J. GeoMech. 8, 105–113.

Wheeler, S.J., Naatanen, A., Karstunen, K., Lojander, M., 2003. An anisotropic elastoplastic model for soft clays. Can. Geotech. J. 40, 403–418.
Whittle, A.J., Kavvadas, M.J., 1994. Formulation of MIT-E3 constitutive model for overconsolidated clays. J. Geotech. Eng. 120, 173–198.
Wood, D.M., 1990. Soil Behaviour and Critical State Soil Mechanics. Cambridge University Press, Cambridge, UK.
Yang, C., Chen, H., Li, J., 2020. Drained cylindrical cavity expansion analysis in anisotropic soils considering 3D strength. Géotech. Lett. 10, 1–7.
Yang, M., Seidalinov, G., Taiebat, M., 2019. Multidirectional cyclic shearing of clays and sands: evaluation of two bounding surface plasticity models. Soil Dynam. Earthq. Eng. 124, 230, 25.
Yao, Y.P., Wang, N.D., 2014. Transformed stress method for generalizing soil constitutive models. J. Eng. Mech. 140, 614–629.
Yin, Z.Y., Chang, C.S., Karstunen, M., Hicher, P.Y., 2010. An anisotropic elastic-viscoplastic model for soft clays. Int. J. Solid Struct. 47, 665–677.
Yu, H.S., 2020. Cavity Expansion Methods in Geomechanics. Kluwer Academic Publishers, Dordrecht, The Netherlands.
Yu, H.S., Houlsby, G.T., 1991. Finite cavity expansion in dilatants soils: loading analysis. Geotechnique 41, 173–183.
Zhang, J., Li, L., Sun, D., 2020. Similarity solution for undrained cylindrical cavity contraction in anisotropic modified Cam-clay model soils. Comput. Geotech. 120, 103405.
Zhao, C., Wang, Y.B., Zhao, C., Wu, Y., Fei, Y., 2020. Analysis of drained cavity unloading-contraction considering different degrees of intermediate principal stress with unified strength theory. Int. J. GeoMech. 20, 04020086.
Zhou, H., Kong, G.Q., Liu, H.L., Laloui, L., 2017. Similarity solution for cavity expansion in thermoplastic soil. Int. J. Numer. Anal. Model. 42 (2), 274–294.
Zhou, H., Wang, Z.L., Liu, H.L., Ding, X.M., 2020. Undrained cylindrical and spherical cavity expansion in elastic-viscoplastic soils. Can. Geotech. J. 58 (10), 1543–1557.
Zhou, H., Liu, H.L., Wang, Z., Ding, X.M., 2021. A unified and rigorous solution for quasi-static cylindrical cavity expansion in plasticity constitutive models. Comput. Geotech. 135, 104162.

Dr. Pin-Qiang Mo obtained his BEng degree in Civil Engineering from China University of Mining and Technology, Xuzhou, China, in 2009, his MSc degree in Civil Engineering from The University of Nottingham, UK, in 2010, and his PhD in Geotechnical Engineering from The University of Nottingham, UK, in 2014. He is now an Associate Research Scientist at State Key Laboratory for Geomechanics and Deep Underground Engineering, China University of Mining and Technology. His research interests include (1) Cavity expansion solutions and their geotechnical applications; (2) Cone penetration testing and bearing capacity of pile foundations; (3) Soil-structure interactions in tunnelling and underground engineering; and (4) Granular material and its mechanics under low gravity condition. He is member of International Society for Soil Mechanics and Geotechnical Engineering (ISSMGE), China Civil Engineering Society (CCES), and Chinese Society for Rock Mechanics and Engineering (CSRME), who also serves as a Scientific Editor of Journal of Rock Mechanics and Geotechnical Engineering (JRMGE). He won the British Geotechnical Association (BGA) Medal in 2016, obtained the Provincial 'Doctor for Innovation and Entrepreneurship' in 2017 and the Provincial Project to support young scientific and technological talents in 2020. He chairs two National Natural Science Foundation of China (NSFC) projects among many others, and has published over 30 peer-reviewed journal papers.